Nuclear Instruments and Methods in Physics Research B 383 (2016) 59–64

Contents lists available at ScienceDirect

Nuclear Instruments and Methods in Physics Research B

journal homepage: www.elsevier.com/locate/nimb

Pattern evolution during ion beam sputtering; reductionistic view

J.-H. Kim, J.-S. Kim *

Department of Physics, Sook-Myung Women's University, Seoul 04310, Republic of Korea

ARTICLE INFO

Article history:
Received 26 November 2015
Received in revised form 8 June 2016
Accepted 9 June 2016
Available online 28 June 2016

Keywords:
Ion beam sputtering
Nano patterning
Growth kinetics

ABSTRACT

The development of the ripple pattern during the ion beam sputtering (IBS) is expounded via the evolution of its constituent ripples. For that purpose, we perform numerical simulation of the ripple evolution that is based on Bradley–Harper model and its non-linear extension. The ripples are found to evolve via various well-defined processes such as ripening, averaging, bifurcation and their combinations, depending on their neighboring ripples. Those information on the growth kinetics of each ripple allow the detailed description of the pattern development in real space that the instability argument and the diffraction study both made in *k*-space cannot provide.

1. Introduction

Extended incidence of energetic ion beam at a surface or the ion beam sputtering (IBS) often results in highly ordered nanometer-scale patterns on various substrates of metals [1,2], semiconductors [3,4], oxides [5,6] and polymers [7]. Typically, near normal incidence of the ion beam leads to the creation of nanodot patterns [8,9]. With the increase of the incidence angle from the surface normal, the patterns composed of the nanometer-scale ripples develop [10,11]. This physically driven self-assembly is easily scalable and cost effective, and thus can be supplementary to the lithography for the applications where the order of the pattern needs not to be addressable [12–15].

The pattern formation by IBS originates from the balance between the mass redistribution near the surface by energetic incident ions and the diffusion of adspecies created during IBS. Bradley and Harper (BH) combined the Sigmund theory of the erosion [16,17] within the linear approximation with the Mullins' model of diffusion of the adspecies [18,19], and put forward the celebrated BH equation [20] or Eq. (1) below. The first two terms on the right hand side (*rhs*) of Eq. (1) lead to the surface instability by curvature-dependent erosion, while the third term represents the diffusion of the adspecies, curing the instability by filling the valley.

$$\frac{\partial h}{\partial t} = -v_x \frac{\partial^2 h}{\partial x^2} - v_y \frac{\partial^2 h}{\partial y^2} - \mathcal{K}\nabla^4 h \tag{1}$$

Fourier transformation of Eq. (1) gives the dispersion relation of the Fourier component of $h(\mathbf{r}, t)$ or $h(\mathbf{k}, \omega_k)$ as shown in Eq. (2).

$$\omega_k = v_x k_x^2 + v_y k_y^2 - \mathcal{K}(k_x^2 + k_y^2)^2 \tag{2}$$

The dispersion relation predicts a generic behavior of the pattern formation governed by BH model; there is a Fourier component $h(\mathbf{k}^*, \omega_{k^*})$ having a characteristic wavelength $\lambda^* = 2\pi/k^* = 2\pi(2\mathcal{K}/v)^{1/2}$ where v means the absolute value of the larger one between v_x and v_y. This component grows most rapidly and governs the pattern in the long run, before non-linear effects become influential in the pattern formation [21,22]. We will call this state as the *characteristic state*.

Since the sputtering is a stochastic process, features of various wavelengths coexist in the early stage of IBS. The transient behavior of those features evolving to form the pattern characterized by λ^* has been studied mainly in *k*-space by the diffraction tools such as the light scattering [23] and the X-ray scattering [24]. However, to the best of our knowledge, the processes leading to the characteristic state have little been microscopically investigated in real space. This is contrasted to the case of the thin film growth where the growth kinetics is described mostly in real space and the atomistic description can even quantitatively reproduce the experimental observations [25,26].

We have delved into the novel approach elucidating the pattern development via the processes by which each constituent of the pattern evolves. Then, the immediate issues are (1) whether there are identifiable processes by which the ripples evolve in the transient states, (2) under which condition each process is realized, and (3) whether the pattern evolution in the transient state can be elucidated in terms of those processes.

* Corresponding author.
E-mail address: jskim@sm.ac.kr (J.-S. Kim).

http://dx.doi.org/10.1016/j.nimb.2016.06.005
0168-583X/

From the numerical simulation, we find that the ripples evolve via various well identifiable processes such as the ripening, averaging, bifurcation, and their combinations. The realization of each process depends not only on the ripple, but on its neighbors. Those processes well elucidate the details of the pattern evolutions observed for the pre-patterned Au(001) surfaces. Thus obtained information should help constructing the microscopic picture for the pattern development that is based on the growth kinetics of the constituent nano structures, and be complementary to the instability argument and the diffraction study both made in k-space.

2. Simulation

We have performed most simulation, employing BH model with the noise term. We have also examined the non-linear effects employing extended Kuramoto Sivashinski (eKS) model as shown below;

$$\frac{\partial h}{\partial t} = -v_x \frac{\partial^2 h}{\partial x^2} - v_y \frac{\partial^2 h}{\partial y^2} - \mathcal{K}\nabla^4 h + \mu_1(\nabla h)^2 - \mu_2 \nabla^2 (\nabla h)^2 + \eta \qquad (3)$$

The coefficients $v_x, v_y, \mathcal{K}, \mu_1$ and μ_2 depend on phenomenological parameters such as flux, ion energy and substrate temperature as well as the substrate. BH equation can be retrieved from eKS equation by neglecting the non-linear terms such as Kadar–Parisi–Zhang (KPZ) [27] and conserved KPZ (cKPZ) terms, respectively the fourth and fifth terms in *rhs* of Eq. (3). KPZ term describes the slope dependence of the sputter yield, to which the saturation of the amplitude is attributed [28]. cKPZ term accounts for the local redeposition of the sputtered material and the surface confined transportation [29]. Any inevitable anisotropy in the nonlinear terms is not included in the Eq. (3). The noise η is represented by an uncorrelated Gaussian distribution with zero mean and a correlator $\langle \eta(\mathbf{r}, t)\eta(\mathbf{r}', t')\rangle = N\delta(\mathbf{r} - \mathbf{r}')\delta(t - t')$, which reflects the stochastic nature of IBS.

For the description of the transient behavior under BH model, we carried out the numerical simulation with $v = 1 (v_x = 1, v_y = 0.01), \mathcal{K} = 1, \mu_1 = 0$ and $\mu_2 = 0$ and $N = 0.01$ in Eq. (3). For eKS model, the following coefficients were taken; $v = 1 (v_x = 1, v_y = 0.01), \mathcal{K} = 1, \mu_1 = 1$ and $\mu_2 = 1$ and $N = 0.01$. Those parameters correspond to the sputtering at the *oblique* angles. The standard system size, lattice constant and time step of our simulation were $L \times L = 256 \times 256, \Delta x = 1$ and $\Delta t = 0.01$, respectively. For the comparison of the simulation with the experimental results, the coefficients with the real physical units were employed as detailed later. Throughout the simulation, the Euler integration method was employed with the improved spatial discretization as suggested by Lam and Shin [30]. Note that the analytic solution of both the linear BH equation [31] and the BH equation with noise term [32] are known. For practical reasons, however, we have made numerical integration of the equations in the present work.

3. Results and discussion

Fig. 1(a–c) show the representative simulated images, respectively, at $t = 5$, 20 and 50, revealing the pattern evolution on initially flat surface according to BH model. In Fig. 1(a), the ripples are frequently interrupted by defects, and undulate irregularly. At $t = 20$, the density of the defects has notably decreased, but the ripples are not straight, yet [Fig. 1(b)]. At $t = 50$, the ripples are almost defect-free, quite straight and have almost uniform width along their ridges [Fig. 1(c)].

Fig. 1(d) shows the power spectral densities (PSDs), i.e., the square of the modulus of the Fourier transform of the surface profile corresponding to Fig. 1(a)–(c). A peak develops centered around the characteristic wave vector $k^* = 2\pi/\lambda^*$ as predicted by the instability of BH model. The peak becomes pronounced with time, indicating that ripples in the pattern become more homogeneous with ever smaller distribution of their wavelengths around λ^*. The temporal evolution of the individual ripple during the transient state and its contribution to the realization of the characteristic state, however, remain obscure.

In order to investigate the growth kinetics of the individual ripple in the transient states, we perform the numerical simulation, starting from various ripple configurations in which the ripples are possibly situated during their temporal evolution in real experiments. Each configuration is represented by a pattern in which two different ripples alternate; Fig. 2(a and b) show two configurations where two kinds of ripples having the same amplitude ($A_1 = A_2$), but with different wavelengths ($\lambda_1 \neq \lambda_2$) alternate. In Fig. 2(a) where $\lambda_1 = 0.79\lambda^*$ and $\lambda_2 = 1.12\lambda^*$, the wavelengths of the two ripples converge to their mean value, $(\lambda_1 + \lambda_2)/2$ as t increases, or *averaging* of the ripples occurs. (From now on, the wavelength of the individual ripple is defined by the valley to valley distance in the line profile across its ridge.).

In Fig. 2(b) where $\lambda_1 = 0.45\lambda^*$ and $\lambda_2 = 0.67\lambda^*$, two adjacent ripples coalesce into one large ripple with its wavelength, $\lambda_1 + \lambda_2$. We will call this process as the *ripening* of the ripples.

Fig. 2(c) show the evolution of an initial surface in which the ripples with the same wavelength ($\lambda_1 = \lambda_2 = 0.67\lambda^*$), but of two different amplitudes ($A_1 = 0.8A_2$) alternate. As IBS proceeds, the ripples with the relatively small amplitude gradually dwarfen, while the large ones grow taller and wider. In the long run, the large ripples become two times wide by taking the space of the disappearing small ripples. This is another form of the ripening of the ripples.

For the uniform ripple pattern with $\lambda = 1.8\lambda^*$ in Fig. 2(d), the cleavage develops at the center of each ripple along its ridge with increasing t [Fig. 2(d-1)], and becomes deeper and then completely

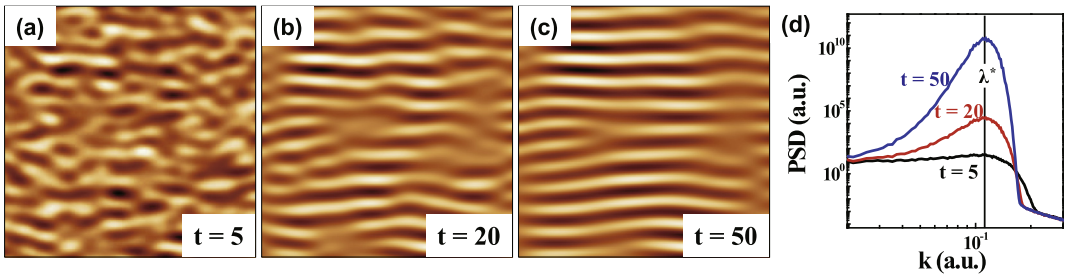

Fig. 1. Patterns developing from initially flat surface according to BH model with $v = 1 (v_x = 1, v_y = 0.01), \mathcal{K} = 1, \mu_1 = 0$ and $\mu_2 = 0$ and $N = 0.01$ in Eq. (3): at (a) $t = 5$ (simulation time), (b) $t = 20$, and (c) $t = 50$. (d) Corresponding PSD curves from the simulated patterns at different times. The peak in the PSD corresponds to the characteristic wave vector $k^* = 2\pi/\lambda^*$.